

Structure of Composites Prepared via Polypyrrole Synthesis in Supercritical CO₂ on Microporous Polyethylene¹

L. N. Nikitin^a, M. O. Gallyamov^b, A. Yu. Nikolaev^b, E. E. Said-Galiyev^a,
A. R. Khokhlov^a, S. S. Bukalov^a, G. I. Magdanurov^a, V. V. Volkov^c,
E. V. Shtykova^c, K. A. Dembo^c, and G. K. Elyashevich^d

^a Nesmeyanov Institute of Organoelement Compounds, Russian Academy of Sciences,
ul. Vavilova 28, Moscow, 119991 Russia

^b Faculty of Physics, Moscow State University,
Leninskie gory, Moscow, 119992 Russia

^c Shubnikov Institute of Crystallography, Russian Academy of Sciences,
Leninskii pr. 59, Moscow, 119991 Russia

^d Institute of Macromolecular Compounds, Russian Academy of Sciences,
Bol'shoi pr. 31, St. Petersburg, 199004 Russia
e-mail: lnik@ineos.ac.ru

Received December 6, 2005;

Revised Manuscript Received March 14, 2006

Abstract—The synthesis of polypyrrole in supercritical carbon dioxide in the presence of the microporous polyethylene has been studied. Formation of polymer composites based on polypyrrole and polyethylene has been demonstrated. The structure of the test samples has been investigated by vibrational spectroscopy, SAXS, and atomic force and scanning electron microscopy. It has been discovered that the oxidized structure of polypyrrole forms during the synthesis under supercritical conditions.

DOI: 10.1134/S0965545X06080098

Recent years have seen the growth of interest in the development of new synthetic procedures, characterization, and search for potential application areas of conducting polymers, such as polyacetylene, polyaniline, polypyrrole, polythiophene, polyphenylene, and polyphenylenevinylene [1, 2]. Among these polymers, polypyrrole holds a peculiar position owing to its high chemical resistance, good conductivity, and other technologically useful properties. Moreover, this polymer offers promise as an active component of membranes, electrochemical sensors, and electrode materials [2, 3]. Therefore, polypyrrole was chosen as the basic object of research in this study.²

However, it should be emphasized that polypyrrole suffers from poor mechanical characteristics (low strength and high brittleness) and cannot form high-strength films. The most promising way of solving this problem and designing new materials is the development of various polypyrrole-based composites.

A mechanically stable and elastic porous film with the deposited polypyrrole layer may be regarded as an ideal system for the practical application of valuable characteristics of a composite, which include conducting, gas-separating, ion-exchange, and other properties. Attempts have been made to prepare composites on the basis of PP [4], crosslinked polystyrene [5], and PI [6] as well as on the surface of the Neosepta AM membrane [7]. However, when the rigid-chain polypyrrole was deposited on these supports, the resultant materials acquired the brittle behavior. Moreover, exfoliation of the coating was observed. In the cited studies, layers were deposited through the oxidative polymerization of pyrrole on polymer supports.

The microporous PE has a great potential as a material for elastic supports. The composite material resulting from the incorporation of polypyrrole combines the high strength and elasticity inherent to the support with the possibility of controlling such characteristics as permeability, ion-exchange behavior, and thermal sta-

¹ This work was supported by the Russian Foundation for Basic Research (project nos. 04-03-32311, 04-03-32229, 04-03-39012, 04-03-32879, and 04-03-32297), Russian Academy of Sciences (grants within the framework of complex programs of the Division of Chemistry and Materials Sciences, Russian Academy of Sciences, "Creation and Study of Macromolecules and Macromolecular Structures of New Generations" and "Creation of New Metallic, Ceramic, Glassy, Polymer, and Composite Materials"), NATO (projects SfP 977998 and CBP.NR.RIG.981306), and a grant from the president of the Russian Federation for Leading Scientific Schools (NSh-1765.2003.3).

² As will be shown below, polypyrrole synthesized in supercritical carbon dioxide is characterized by an increased oxidation degree; however, in what follows, we will use the term polypyrrole rather than oxidized polypyrrole as a matter of convenience.

bility [8] via variation of the content of the conducting component in the system. The polymerization is carried out from the gas phase of the monomer [9].

Considerable progress has been achieved in the development of engineering processes based on the use of supercritical fluids, especially supercritical carbon dioxide [10–12]. This is a cheap, flameproof, nontoxic, and ecologically safe medium having rather low critical parameters (the critical temperature $T_{cr} = 31.1^\circ\text{C}$, the critical pressure $p_{cr} = 7.29$ MPa, and the density $\rho_{cr} = 0.47$ g/cm³). At present, many polymers, including the conducting polypyrrole [13], have been synthesized by polymerization and polycondensation processes in supercritical CO₂. Polyurethane–polypyrrole foams were obtained with the use of supercritical CO₂, and their properties have been investigated. Conducting foams were prepared via the two-stage scheme involving pyrrole diffusion from the gas phase into the foamlike polyurethane and subsequent polymerization [14, 15]. We first studied the synthesis of composite materials based on the microporous PE and polypyrrole in supercritical CO₂ [16, 17]. The elaboration of synthetic procedures for similar composites in supercritical CO₂ on the microporous PE offers considerable promise since, owing to the presence of pores and through channels, the continuous phase of the conducting polymer may be formed in the bulk of the porous support and a highly developed relief of the surface ensures fixation of the polypyrrole being formed [8, 9, 18].

In this study, we comprehensively examined possibilities for controlling the structure of composite materials based on the microporous PE with lower and higher orientation degrees (PE-1 and PE-2, respectively) and polypyrrole formed in supercritical CO₂. The structure of the starting PE-1 and PE-2 films and of the resultant composites was studied by microscopy, spectrometry, and X-ray scattering.

EXPERIMENTAL

Materials and Techniques

Carbon dioxide [GOST (State Standard) 8050-85] had a purity of 99.998% (OAO Balashikha Compressor Plant, Linde Gas AGA, Balashikha). According to the certificate, the volume fraction of moisture in CO₂ was no more than 5×10^{-6} vol %. In addition, we used pyrrole-2-carboxylic acid (PCA, Aldrich, 99%), anhydrous ferric trichloride (Merck, 98%), and methanol (Khimmed, anhydrous, 99.8%); all these substances were used as received.

PE-1 and PE-2 films were prepared from HDPE with $M_w = 1.4 \times 10^5$ and a melting temperature of 132°C as described in [19]. PE samples were extruded at 200°C, annealed at 130°C for 30 min, and then subjected to uniaxial extension (in a different mode for PE-1 and PE-2). In the course of extension, pore formation took place. The as-prepared porous films were

thermally fixed at 115°C. The thickness of the porous film was 10–15 μm, and micropore size was 50–600 nm. The porosity of the material achieved 40–50%, and its density was 0.59 ± 0.05 g/cm³. The synthesis of polypyrrole on PE-1 and PE-2 was carried out in supercritical carbon dioxide at a pressure of 10.0–30.0 MPa in the temperature range 60–120°C.

Synthesis of Polypyrrole in the Presence of Microporous PE

The composites were prepared in ~20-cm³ stainless steel reactors that were placed in a thermostat equipped with a programmable temperature regulator and a magnetic stirrer. The microporous PE film was placed over a stirrer on a stainless steel grid holder to avoid stirrer–film contact in the course of synthesis. A PCA weighed portion (0.03 g) was placed on the bottom of the reactor. Pressure was created with the use of the pressure generator (High Pressure Equipment Company, USA).

The standard procedure of preparing microporous PE–polypyrrole composites involved the oxidative polymerization of PCA on the microporous PE and included several stages. At the first stage, the PE film was soaked in the oxidizer solution (0.5–4.0 mol/l methanolic solution of FeCl₃) with subsequent drying for several minutes. The second stage consisted in the thermal decarboxylation of PCA on the microporous PE matrix impregnated with the oxidizer and the preparation of polypyrrole. At this stage, the PCA weighed portion and the film of the microporous PE were loaded in the reactor and sealed hermetically and the temperature and pressure were raised to the preset values. The synthesis time was 0.5–4 h. At the final stage, ferric chloride uninvolved in the reaction was removed from the composite. To this end, the composite was washed with methanol and methanol was then removed via drying the product in air at 80–90°C to a constant weight.

For polypyrrole, anal. calcd. (%): C, 71.6; H, 7.5, N, 20.9.

Found for polypyrrole synthesized in supercritical CO₂ (%): C, 54.25; H, 4.3; Fe, 2.06; N, 11.92; Cl, 10.20; O, 17.27 (the latter value was obtained by subtracting the sum of the other elements from 100%).

The thickness of the test samples was measured on an IKV-3 vertical projective optometer. The measurement error was ± 0.2 μm.

Analytic Procedures and Instruments

Spectroscopic studies of the composites were performed by the ATR FT-IR spectroscopy on a Thermo Nicolet Nexus FT-IR spectrometer (a resolution of 0.5 cm⁻¹, and a scan number of 64). Measurements were made with a ZnSe crystal at an incident angle of 45°. The spectral range was 650–4000 cm⁻¹.

The synthesis of polypyrrole in supercritical CO₂ was monitored by laser confocal Raman scattering

microscopy. This method is useful for measuring spectra from various probed regions situated not only near the surface but also in the bulk of the sample. The Raman spectra of the parent and composite samples were taken on a Jobin-Yvon LabRAM laser microspectrometer equipped with a microscope and a video camera. A He-Ne laser operating at a wavelength of 632.8 nm was used. The power of the exciting Raman radiation was 0.15–1.5 mW.

Contact mode atomic force measurements were performed on a Nanoscope IIIa (Digital Instruments, USA) scanning probe microscope in the constant-force mode.

AFM images were plotted with the use of the Femtoscan Online 1.6 software (the Advanced Technologies Center, Russia) [20].

SEM images of the microporous PE and the composites were taken on a DMS 962 (Carl Zeiss, Germany) scanning electron microscope.

SAXS studies were carried out on an AMUR-K homemade diffractometer (designed at the Special Design Bureau of the Shubnikov Crystallography Institute, Russian Academy of Sciences) according to the Kratky method [21]. Measurements were made using CuK_α radiation with a wavelength of 0.154 nm. The wave vectors were $s = 0.12\text{--}5.5 \text{ nm}^{-1}$ ($s = 4\pi\sin\theta/\lambda$, where 2θ is the scattering angle). The radiation source was a BSV-29 fine-focus X-ray tube equipped with the copper anode. The operating voltage was 30 kV, and the current was 30 mA. An OD-2 linear position-sensitive detector with 1850 working channels in the measurement range was designed at the Budker Institute of Nuclear Physics of the Siberian Division of the Russian Academy of Sciences. The sample-to-detector distance was 700 mm, the measurement time was 3000 s, and pyrolytic graphite was used as a monochromator.

Collimation was performed according to the Kratky scheme with a slit width of 0.2 mm and a length of 8 mm. The sample thickness was variable; therefore, no absolute calibration was made. The scattering intensity curve recorded for the empty sample holder was subtracted from the corresponding curve taken for the test sample. The former curve corresponds to scattering from air in the sample chamber, slit edges, and the Lavsan film that seals the vacuum chamber entrance. The experimental data were normalized to the incident beam intensity, and then correction for collimation distortions due to beam slit collimation in the Kratky collimator was introduced. The test microporous PE and composite samples were stacked in piles consisting of eight layers and were arranged so that the direction of film orientation was equal for all layers and perpendicular to the incident beam. The experiments demonstrated that the pattern of SAXS curves remains invariable with the turn of the film in the plane perpendicular to the beam. Evidently, the orientation of pores makes

itself evident in the case of sizes larger than the sizes of scattering heterogeneities contributing to scattering at the test scattering angles (an angle at $s = 0.12 \text{ nm}^{-1}$ corresponds to a size of 52 nm).

In order to analyze the size distribution of structural heterogeneities in the test sample, two independent methods were employed to interpret the SAXS data from size distribution curves of scattering heterogeneities under the assumption that their shape is spherical. This approach makes it possible to estimate the typical sizes (equivalent sizes and radii of gyration) of heterogeneities in samples with disordered pores and inclusions. The first method consists in computing volume size distribution $D_V(R)$ on the assumption that scattering particles are spherical in shape through the formula

$$I(s) = (\Delta\rho)^2 \int_{R_{\min}}^{R_{\max}} D_V(R) m^2(R) i_0(sR) dR. \quad (1)$$

Here, R is the radius of a sphere; R_{\min} and R_{\max} are the minimum and maximum radii; and $i_0(x) = \{[\sin(x) - x\cos(x)]/x^3\}^2$ and $m(R) = (4\pi/3)R^3$ are the form factor of the sphere and its volume, respectively. In $D_V(R)$ calculations, R_{\min} was taken as zero and R_{\max} was selected individually for each particular case as the minimum value that provides the mean-square deviation of the theoretical curve calculated by formula (1) of no more than 1.8 (a theoretical deviation of 1.0 is unattainable because of the presence of weak systematic intensity deviations against the background of random measurement noises at almost the same amplitude).

The second approach is based on the direct simulation of SAXS intensity by the linear combination of scattering from polydisperse particles. Spherical bodies were also chosen as particles. Small-angle scattering from a system consisting of K fractions of polydisperse components was presented as a sum of partial intensities $I_{k0}(s)$ of scattering from their components weighed according to their volume fractions V_k :

$$I(s) = \sum_{k=1}^K V_k I_{k0}(s).$$

Here, the intensity of scattering from the components is

$$I_{k0}(s) = \int_0^\infty D_k(R) v_k(R) [\Delta\rho_k(R)]^2 i_{0k}(s, R) dR,$$

where $\Delta\rho_k(R)$, $v_k(R)$, and $i_{0k}(s, R)$ designate the electronic contrast, volume, and normalized intensity of scattering (the form factor) for a particle with radius R , respectively. The volume distribution functions $D_k(R)$ were presented as the Schultz distribution described by

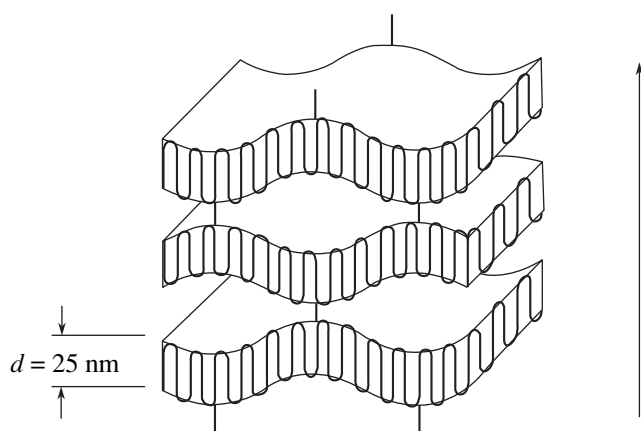


Fig. 1. Schematic presentation of the microporous PE structure: d is the size of folded lamellae, the arrow denotes the orientation direction, and the solid lines designate chain bridges connecting lamellae.

two parameters, the mean value of R_{0k} and the dispersion ΔR_k :

$$D_k(R) = G(R, R_{0k}, \Delta R_k) \\ = \left(\frac{z+1}{R_{0k}}\right)^{z+1} \frac{R^z}{\Gamma(z+1)} \exp\left[-\frac{(z+1)R}{R_{0k}}\right]$$

$$(z = (R_{0k}/\Delta R_k)^2 - 1).$$

The sought parameters in this approach are the mean radii, dispersion, and volume fraction of each mixture component. These parameters were sought with the use of the POLYMIX software derived from the MIXTURE program [22].

RESULTS AND DISCUSSION

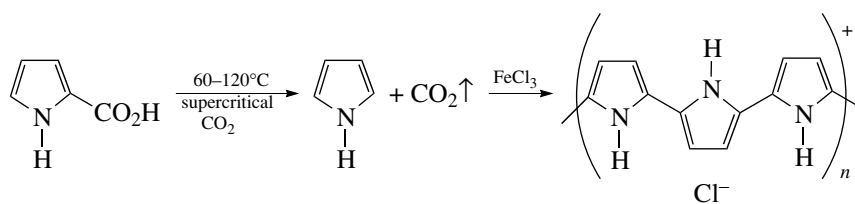
As was mentioned above, formation of the oriented porous structure of porous PE films was completed by an increase in orientation during uniaxial extension of

the annealed samples at the stage of pore formation [23, 24], where discontinuities—pores—appear as a result of moving apart and bending of lamellae situated between bridges composed of tie chains connecting them. In the course of thermal fixation, stabilization of the porous structure occurred owing to the removal of inner stresses upon prolonged storage of the samples at high temperatures [25]. The structure of the microporous PE film samples is schematically presented in Fig. 1 [26]. Pore formation in these samples proceeds during uniaxial extension and may be controlled by the degree of this extension, that is, the degree of orientation of the sample. PE-1 and PE-2 with lower and higher orientation degrees, respectively, were selected as supports. As is shown in Fig. 1, the structure comprises a system of folded-chain crystals (lamellae) arranged parallel to each other and connected by stressed-tie chain bridges.

SEM and AFM measurements (Fig. 2) show that the films are characterized by a strongly developed relief surface with a typical lateral relief size of 0.5–2.0 nm which increases with the degree of orientation of the sample (cf. Figs. 2a and 2b, 2c and 2d).

AFM images measured for the surface of microporous PE samples (Figs. 2c, 2d) demonstrate dark regions located between structures forming the surface relief. These regions designate localization of pores of various depths. Figure 2 shows that the surface relief preserves the lamellar structure of the porous sample (Fig. 1) at a larger scale level (the lamellae are of the order of 25 nm in size) and on the whole is in agreement with the above-described model concepts concerning pore formation in PE. In the course of polymerization, pyrrole molecules may arrange both on the surface of the microporous PE as well as on the walls of pores and in the intercrystallite space.

The general scheme of reactions giving rise to the formation of polypyrrole under the above-described experimental conditions is outlined below. This scheme includes the thermal decarboxylation of PCA and subsequent oxidative polymerization of pyrrole formed in supercritical CO_2 [13].



Pyrrole resulting from the thermal decarboxylation of PCA is involved in oxidative polymerization initiated by ferric trichloride. The polymerization carried out in supercritical CO_2 in the presence of microporous PE affords a material containing different amounts of polypyrrole. This result is of importance for further application of composites in various processes. We pro-

posed that the amount of polypyrrole incorporated into the microporous PE may be controlled by an increase in its content in the pores and on the surface of PE. With this aim in view, several polypyrrole syntheses on the microporous PE were accomplished in series; that is, after the first synthesis of polypyrrole, the PE film was again treated with ferric trichloride and the polypyrrole

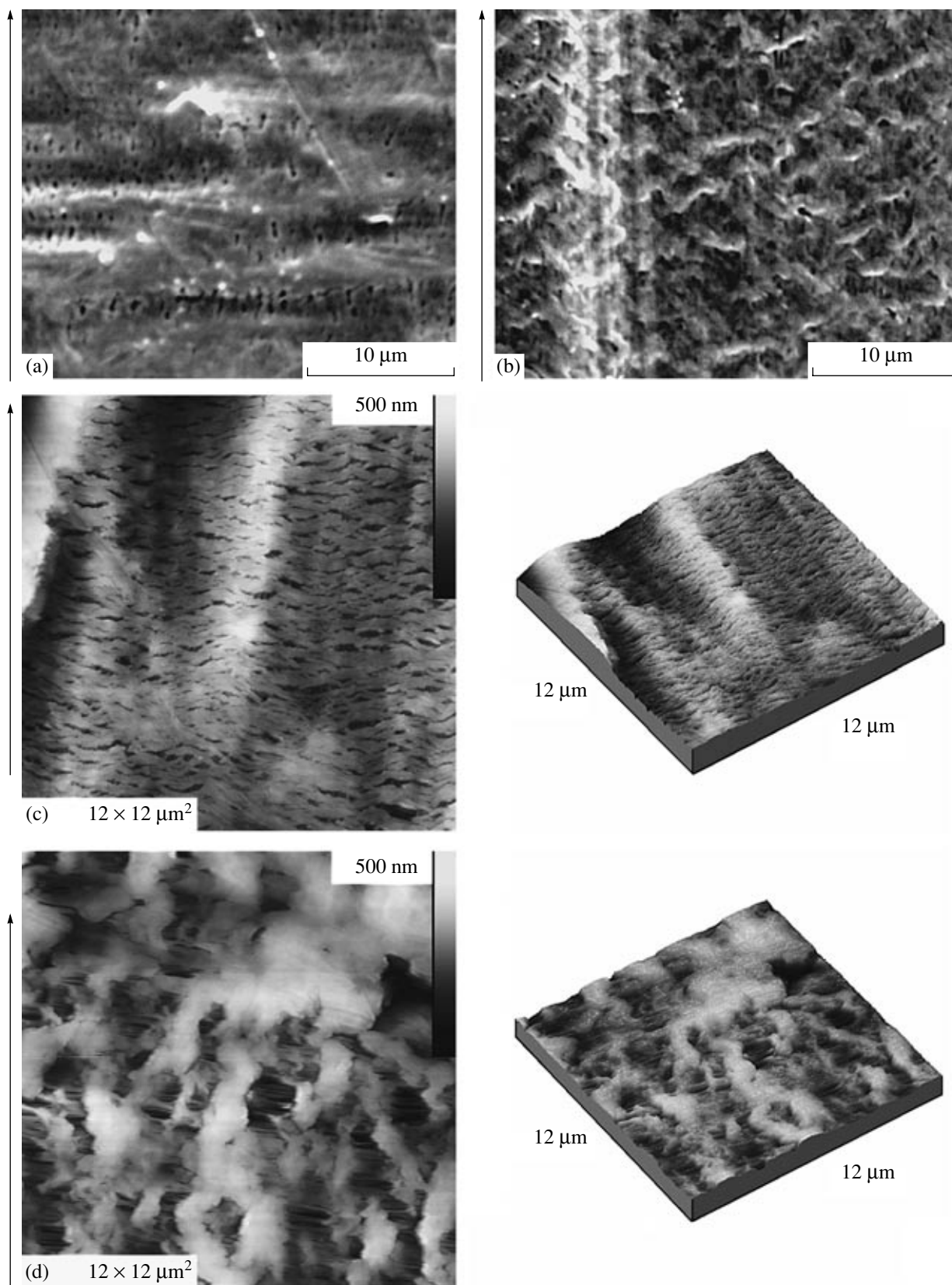


Fig. 2. Panels: (a, b) SEM micrographs. Panels (c, d): AFM images of the surface structure of PE-1 and PE-2. The arrow denotes the orientation direction.

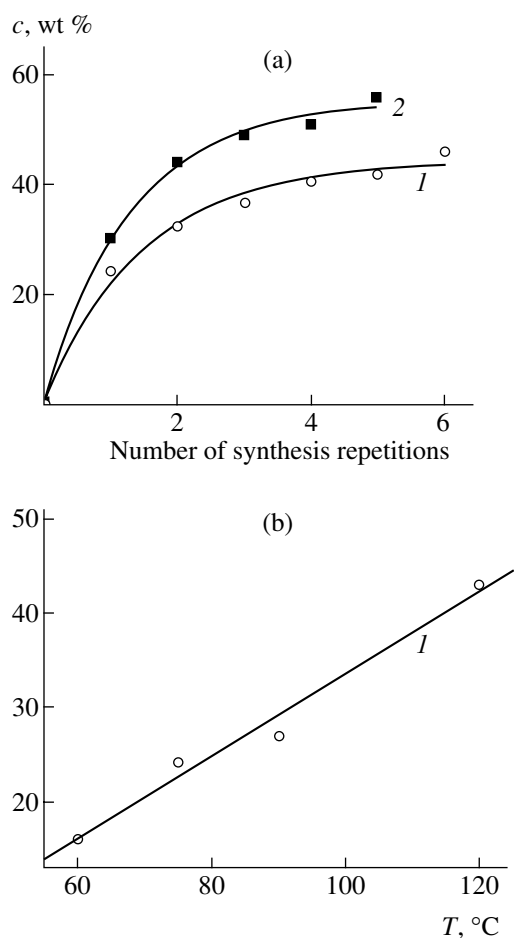


Fig. 3. The content c of polypyrrole incorporated into the composite vs. (a) the number of syntheses and (b) temperature. (1) PE-1 and (2) PE-2. The conditions of polypyrrole synthesis: 20 MPa, 75°C, 2 h, and soaking in a FeCl_3 solution in methanol (1 mol/l).

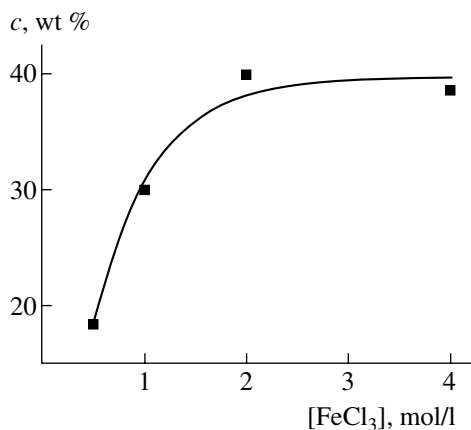


Fig. 4. The content c of polypyrrole incorporated into the composite based on PE-2 vs. the concentration of ferric chloride in methanol for the single synthesis. The synthesis conditions: 20 MPa and 2 h.

layer was obtained anew on the film. Usually, after four to six cycles, evident signs of polypyrrole exfoliation from the film were detected. Therefore, it was unreasonable to further increase the amount of polypyrrole. The weight content of polypyrrole in the composite was calculated with the formula

$$X = (M_c - M_{\text{PE}})/M_c,$$

where M_c is the weight of a composite and M_{PE} is the weight of PE.

The content of polypyrrole in the composite depends on the number of synthesis repetitions and temperature and slightly depends on pressure (within 10.0–30.0 MPa) and durations longer than 2 h. The content of polypyrrole in the composite nonlinearly increases with the number of syntheses, and after four to six repetitions the growth of this value ceases (Fig. 3a). The nonlinear pattern of this process may be explained by the fact that, during each subsequent synthesis, the porosity of the composite decreases owing to deposition of the polypyrrole layer. Moreover, the content of the FeCl_3 oxidizer added before the next synthesis also drops. As a result, a nonlinear reduction in the weight of the resulting polypyrrole takes place.

The content of the conducting polymer in the composite is affected by the temperature of synthesis and the concentration of ferric chloride in methanol during its diffusion into the microporous PE. Figure 3b plots the content of polypyrrole in the composite as a function of the temperature of synthesis. As the temperature is increased, the content of the added polypyrrole linearly increases up to 120°C. This result provides evidence that the efficiency of thermal decarboxylation increases. A further rise in the temperature of synthesis could lead to the onset of PE melting [27].

As is clear from Fig. 4, the content of the conducting polymer in the composite may also be controlled through variation of the amount of the FeCl_3 oxidizer added to PE from the methanol solution (no more than 2 mol/l). However, a further increase in concentration did not result in an increase in the content of polypyrrole in the composite, other conditions being equal. These results may be rationalized by the fact that, after dissolution of the oxidizer in methanol (at a concentration higher than 2 mol/l), the viscosity of the solution increased. Therefore, its penetration into minute pores was hindered and the weight of the oxidizer in the pores and on the surface of PE declined.

Figure 5 illustrates an increase in the composite thickness with a gain in the content of polypyrrole. It is seen that the thickness of the film based on PE-1 gradually grows with an increase in the content of polypyrrole. For PE-2-based composites, the pattern of this dependence was somewhat different. For the amount of polypyrrole in the PE-2-based composite below ~32–35%, no marked increase in the composite thickness is observed. This is apparently related to the predominant

filling of inner cavities and pores of PE-2 whose volume in this sample is higher than that in the case of PE-1. Subsequently, the thickness of the composite increases with a rise in the content of polypyrrole at a much higher rate since its layer develops on the composite surface that has already been formed. As is seen from Fig. 5, there is significant scatter in the thicknesses of the composites under study. Therefore, the curves were plotted for measured thicknesses at ten different points and averaged measurement data.

The feasible mechanism invoked to describe formation of the polypyrrole phase consists in the initial partial filling of pores available in PE. As a result, their contribution to scattering diminishes and the relative content of pores with a mean size of 30 nm decreases. A rise in the fraction of pores with a size of 10 nm is related to the fact that the pores with these sizes are weakly filled with polypyrrole. Simultaneously, an increase in the contribution of large heterogeneities to scattering suggests the appearance of large polypyrrole clusters in both the bulk of the microporous PE and on its surface. A change in the size distribution curves indicates that polypyrrole partially fills the pores of the parent PE. No change in the small-angle X-ray scattering profile should be observed if the polypyrrole film forms on the surface. At the same time, close electron densities of polyethylene and polypyrrole prevent a more comprehensive gain of insight into the morphology of one polymer embedding into the other one.

The conclusion concerning the gradual build-up of the polypyrrole layer on the composite surface is confirmed by Raman scattering, AFM, and electron microscopy measurements. Figure 6 presents the Raman spectra as a function of the number of synthesis repetitions for samples with different weight contents of polypyrrole in the composite. As is seen, the Raman spectra taken from the surface of the films containing 32–46% polypyrrole are nearly identical. The Raman spectra reported for the neutral and oxidized polypyrroles [28] give us grounds to infer that the spectrum given in Fig. 6 corresponds to the oxidized form of this polymer. Specifically, a broad band at 1600 cm^{-1} is the superposition of bands arising from vibrations of a system of conjugated C=C bonds in the cation radical (polaron) and biradical (bipolaron) resulting from the oxidation of polypyrrole [29]. Bands at 1054 and 984 cm^{-1} correspond to vibrations of the cation radical, and bands at 1082 and 936 cm^{-1} are due to vibrations of a dication in the oxidized polypyrrole fragments [28]. The thickness of the polypyrrole phase in the composite is high enough (~3–5 μm) since no bands are observed in the Raman spectra of PE. This finding implies that, during polymerization on the porous PE film, a rather thick polypyrrole layer that occurs both on the surface and inside the film forms. However, if the amount of polypyrrole on the surface of the PE film is small, very weak bands due to PE appear in the spectrum along

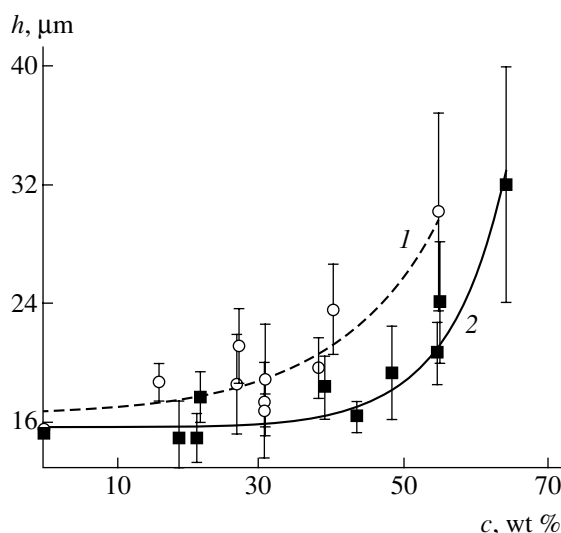


Fig. 5. The film thickness h of the composite vs. the content c of polypyrrole in the samples based on (1) PE-1 and (2) PE-2.

with the bands corresponding to polypyrrole. This circumstance offers an opportunity to estimate the amount of polypyrrole relative to the amount of PE.

The confocal optics allows determination of the amount of polypyrrole during penetration of an exciting laser beam into the film depth (Fig. 7). Curve a is the Raman spectrum of the individual polypyrrole, and curve b is the Raman spectrum of the thin polypyrrole layer on the surface of the PE film (the PE-1-based sample containing ~17% polypyrrole). Even this spectrum exhibits weak bands at 1128 and 1295 cm^{-1} attributed to PE. This spectrum and all subsequent spectra shown in Fig. 7 were normalized to the intensity of the 1128- cm^{-1} band due to PE. As the lens focus moves deep into the sample (curves c – f), the bands due to PE become more and more pronounced. Figure 8 demonstrates the relative intensity of the 1600- cm^{-1} band (relative to the intensity of the 1128- cm^{-1} band due to PE) as a function of the depth of penetration into the sample. Evidently, the content of polypyrrole in PE gradually decreases to a depth of 5 μm and then stabilizes at a certain constant value (Fig. 7, curves g – k). A deeper penetration of the mixture components inside the porous PE film is hindered by their diffusion along the complex shape of strongly twisted pores. Moreover, FeCl_3 and PCA molecules cannot enter into the smallest pores because of geometric obstacles. Therefore, only a limited amount of polypyrrole embeds into PE in the course of the aforesaid synthesis. Thus, when all pores in the bulk of the PE film that are accessible to polypyrrole are filled, next syntheses, regardless of the time and experimental conditions, only give rise to an increase in the thickening of the polypyrrole layer on the film surface without deformation of inner pores of PE.

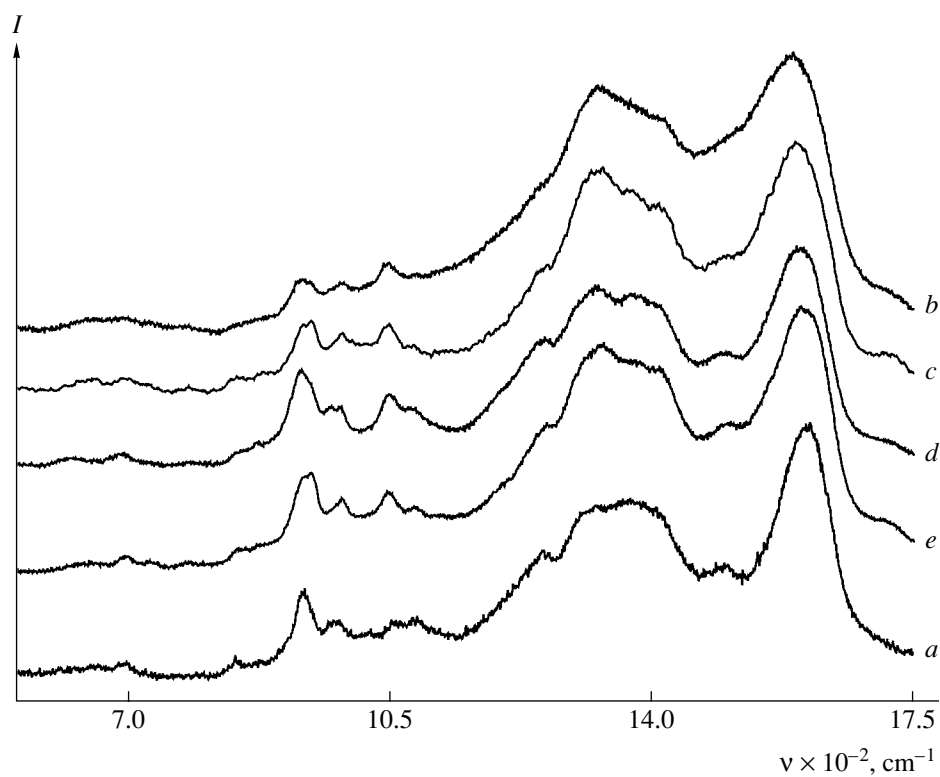


Fig. 6. Raman spectra of (a) polypyrrole and composite samples based on PE-1 with polypyrrole contents of (b) 32.2, (c) 36.6, (d) 40.4, and (e) 45.9%.

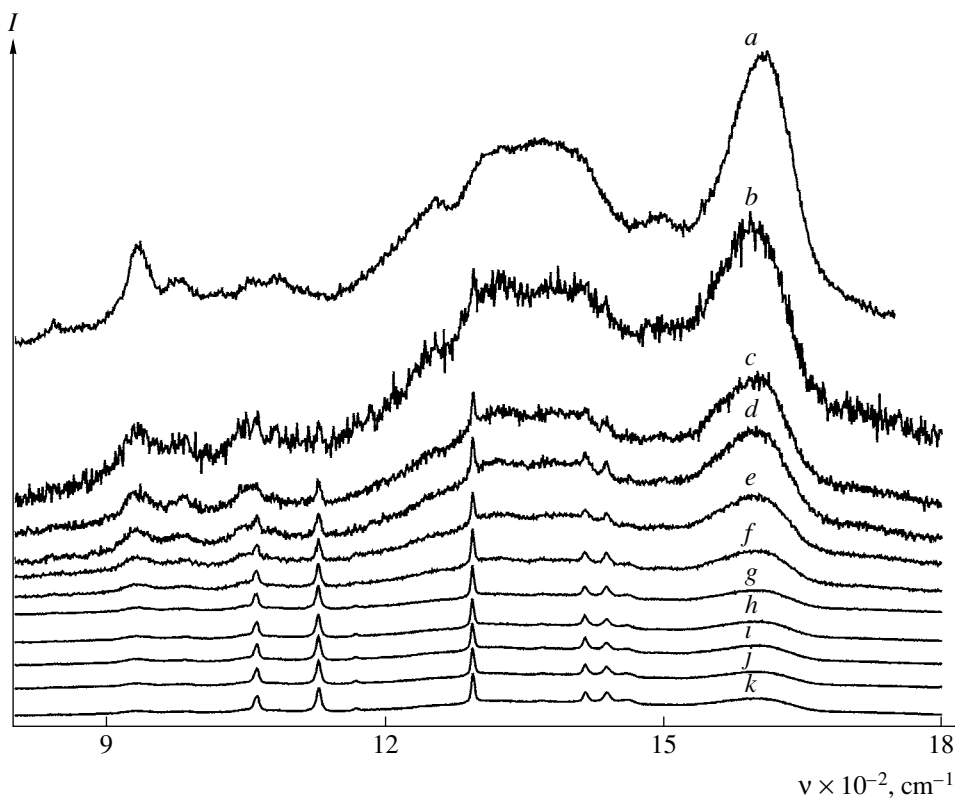


Fig. 7. Raman spectra of (a) polypyrrole and the composite sample containing ~17% polypyrrole over penetration depths of exciting laser radiation of (b) 0, (c) 0.5, (d) 1.0, (e) 1.5, (f) 2.0, (g) 2.5, (h) 3.0, (i) 3.5, (j) 4.0 and (k) 5.0 μm .

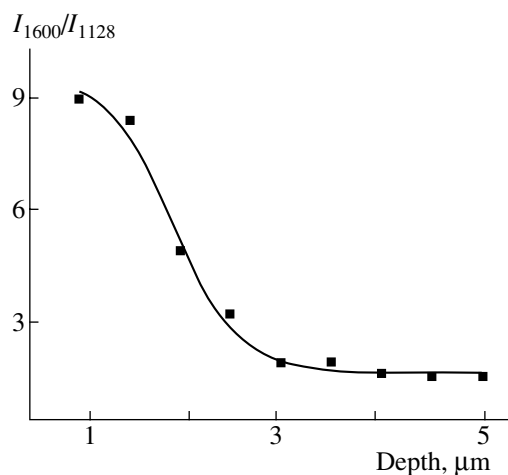


Fig. 8. The relative intensity of the 1600-cm⁻¹ absorption band vs. the penetration depth of exciting laser radiation.

We failed to unambiguously identify the intense broad band at 1250–1450 cm⁻¹, which, according to the published data, does not refer to the spectrum of polypyrrole. With due regard for the technique of composite synthesis, iron compounds may occur in the resulting material. In particular, the Raman spectra of several films exhibit bands that correspond to the intact FeCl₃ (287 cm⁻¹) that was preserved beneath the polypyrrole layer and thus was not removed from the sample during washing and to Fe₂O₃ (221, 400 cm⁻¹) and Fe₃O₄ (651 cm⁻¹) oxides arising from side reactions of ferric chloride with oxygen [30].

The FT-IR ATR spectra of the starting microporous PE and the related composite are shown in Fig. 9. The spectra exhibit absorption bands at 1546 cm⁻¹ (vibrations due to C=C bonds of conjugated regions of polypyrrole chains) and bands at ~1180 cm⁻¹ corresponding to vibrations of C-N groups of polypyrrole.

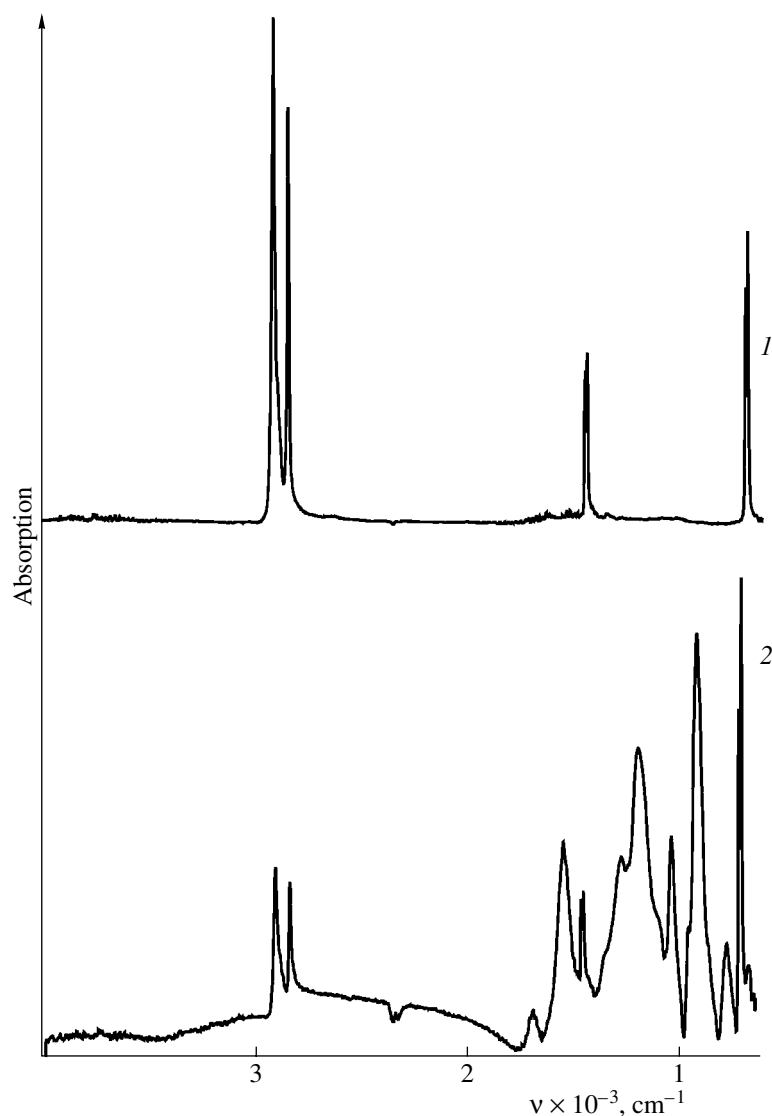


Fig. 9. ATR FT-IR spectra of the starting microporous PE and of the composite based on PE-1 and 18% polypyrrole.

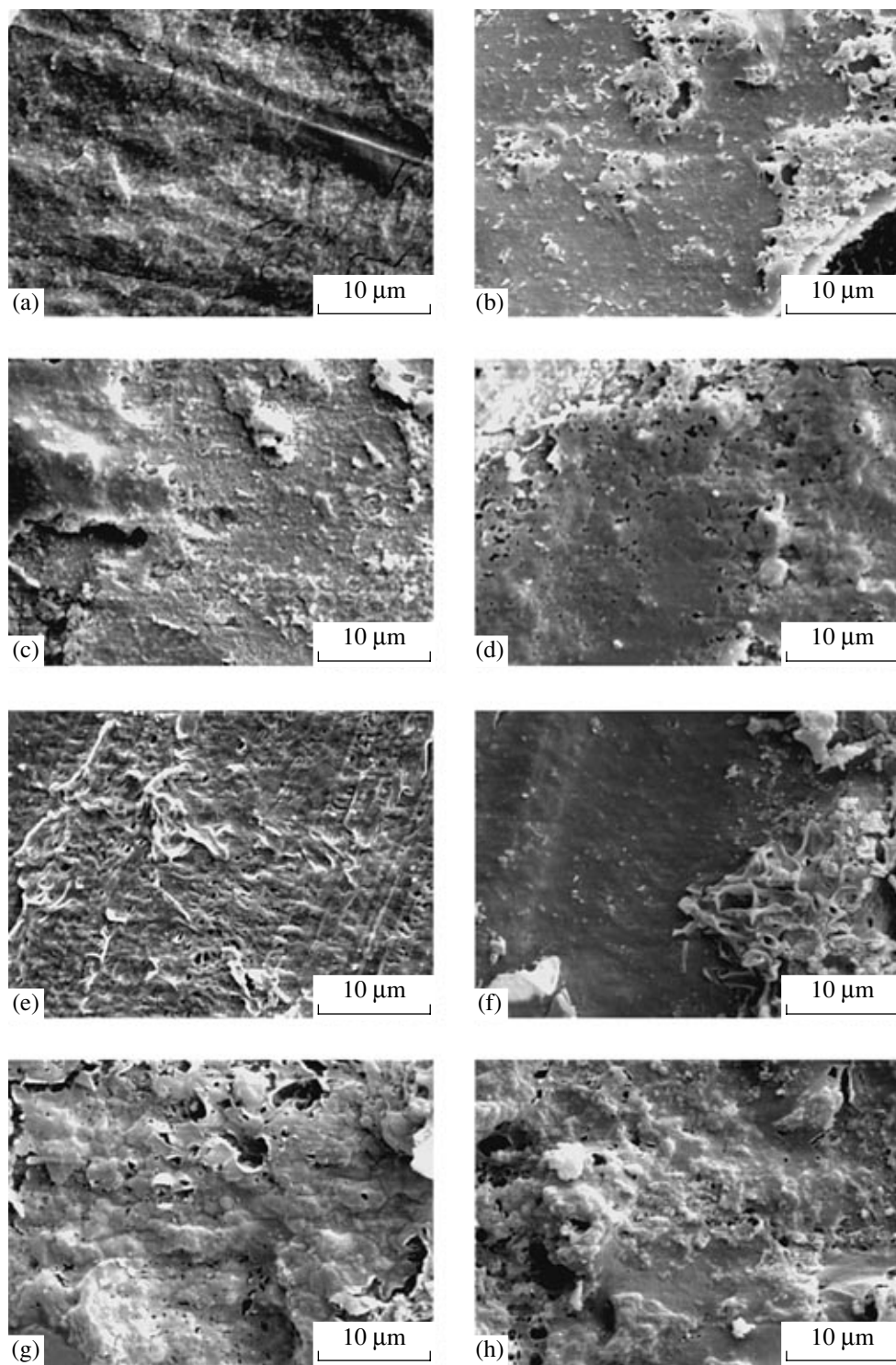


Fig. 10. Electron micrographs of the surface of composite samples based on (a–d) PE-1 and (e–h) PE-2 with polypyrrole contents of (a) 24.2, (b) 32.2, (c) 36.6, (d) 40.4, (e) 29.9, (f) 44.1, (g) 49.0, and (h) 50.9%.

SEM studies of PE-1- and PE-2-based composites containing different amounts of polypyrrole (Fig. 10) demonstrated that, after completion of the first cycle of polypyrrole synthesis, the whole surface morphology of the samples begins to change. However, the initial

structure of the microporous PE still may be traced on some regions of the composite surface.

It is clear that, as the content of polypyrrole in the composite is increased, it begins to penetrate into the pores of PE (Figs. 10a, 10e); then covers some regions

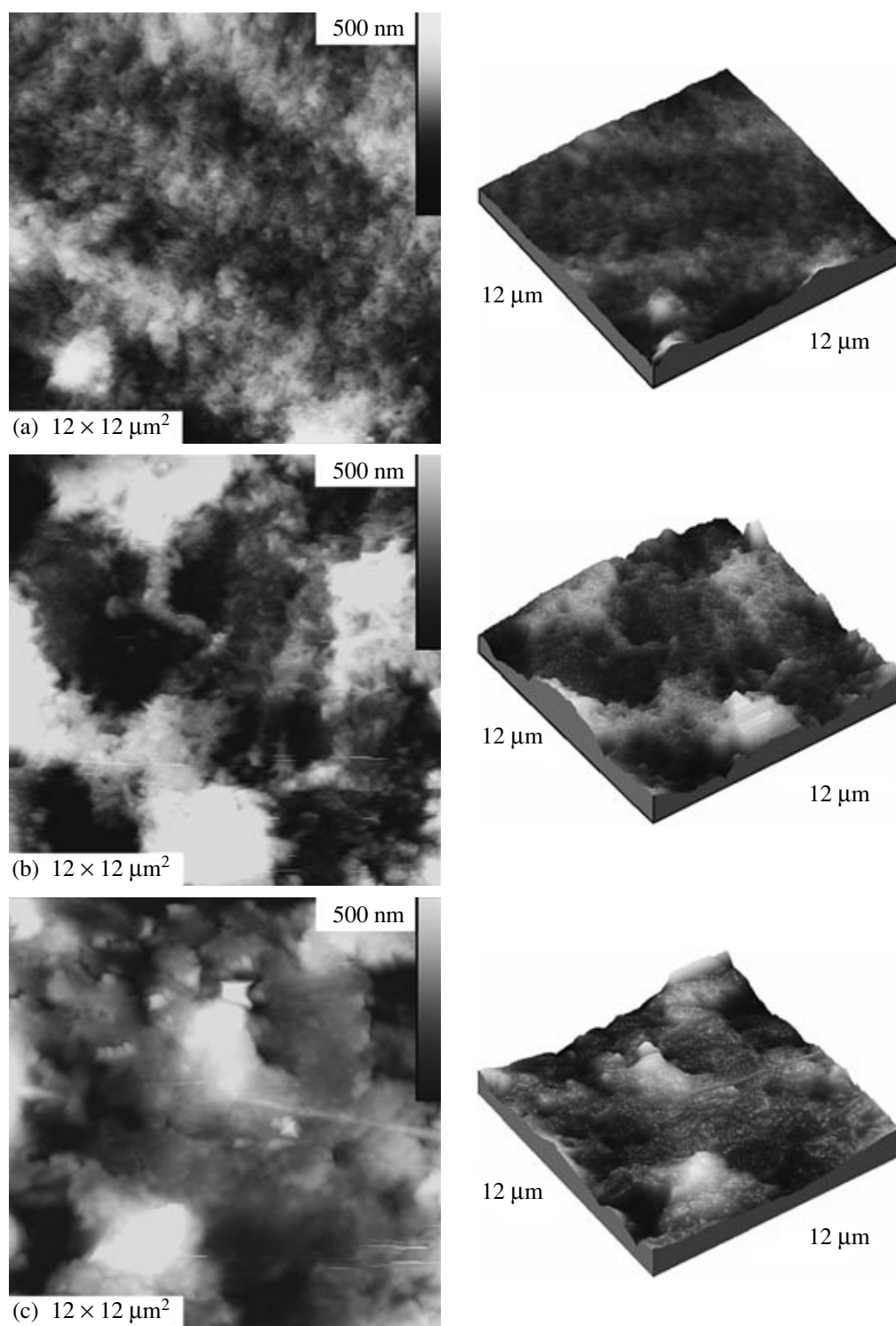


Fig. 11. AFM images of the surface of composite samples based on (a–c) PE-1 and (d–f) PE-2. The polypyrrole contents are (a) 24.2, (b) 36.6, (c) 40.4, (d) 29.9, (e) 44.1, and (f) 49.0%

of the composite surface (Figs. 10 b, 10f); and, finally, forms a layer with a sufficiently nonuniform surface (Figs. 10c, 10d, 10g, 10h). Both heterogeneity and roughness of the composite surface increase with an increase in the number of polypyrrole polymerization

cycles. Seemingly, this is related to the partial mechanical destruction of the formed polymer layer on separate regions of the samples. Sometimes, initial signs of local exfoliation of flakes of the partially destroyed polypyrrole layer may be detected as early as after the

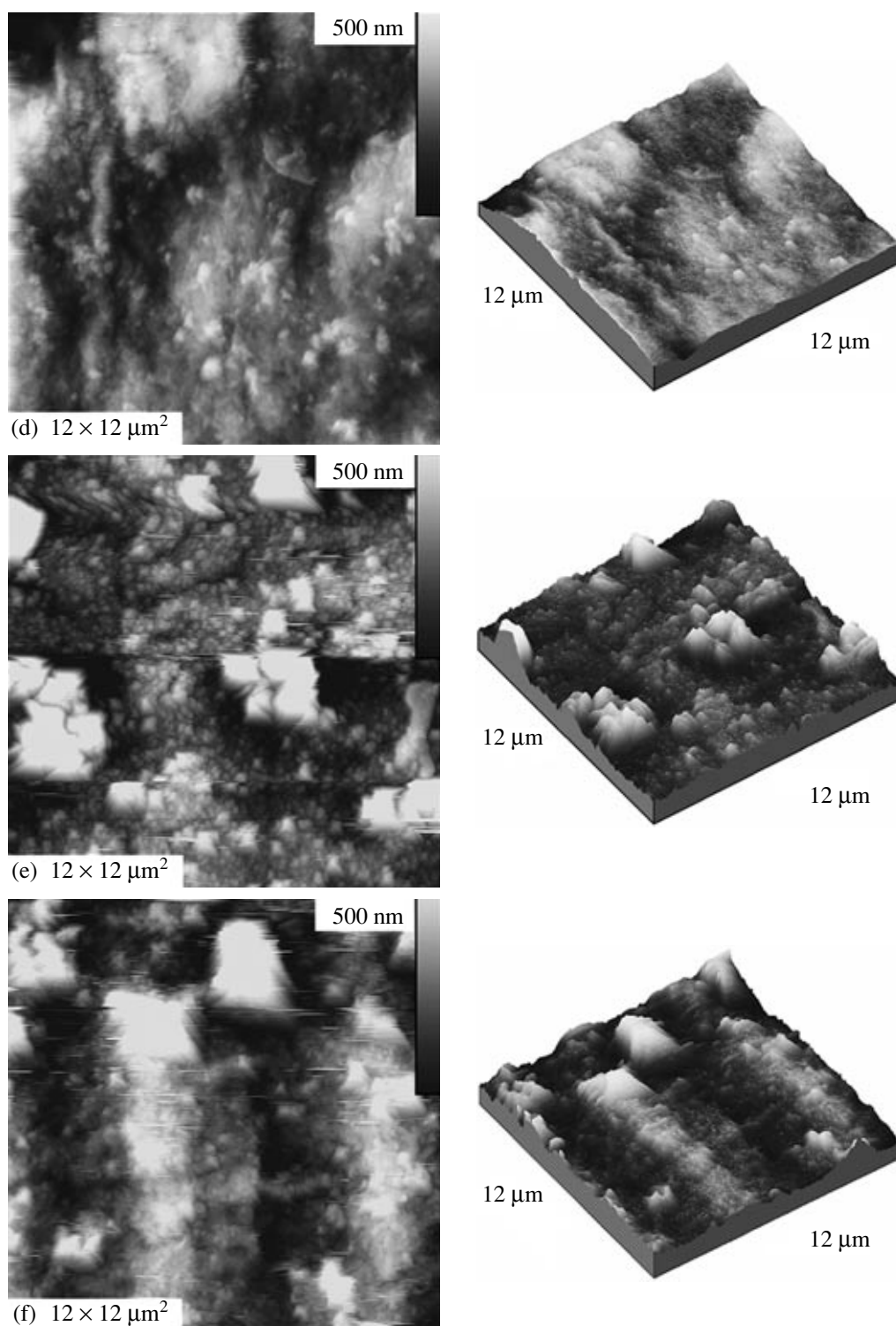


Fig. 11. (Contd.)

first repeated polymerization cycle. However, the local homogeneity of the surface for some regions of the samples could have been enhanced during repetition of synthesis cycles since the structure of the relief of the polymer support surface was masked by a relatively

homogeneous polypyrrole layer (with some defects as small pores).

The SEM data are in agreement with the AFM studies of the composites under consideration (Fig. 11). The AFM technique that provides direct information about

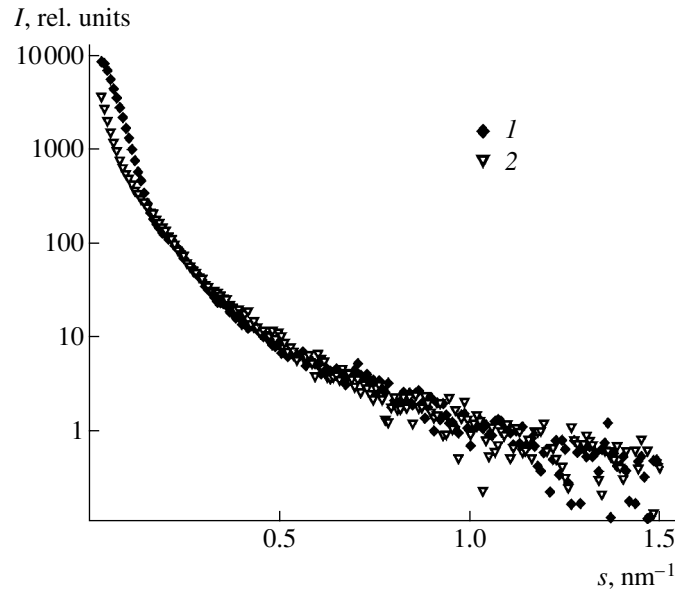


Fig. 12. Scattering curves for (1) starting and (2) composite samples.

the height of surface structures allows us to state that the mean roughness and heterogeneity of the samples grow during the repeated syntheses of polypyrrole. It should be emphasized that the highly developed structure of the sample surfaces, in combination with their certain mechanical instability under the probe edge of the microscope, complicated the AFM measurements of the composites, especially after multiple cycles of pyrrole polymerization.

Figure 12 shows SAXS curves for the starting PE-1 film (curve 1) and the PE-1-based composite containing ~17% polypyrrole (curve 2). As is seen, the experimental small-angle scattering profiles exhibit no peculiar features allowing conclusions regarding the inner structure of the test films since no well-defined Bragg's peaks are detected. However, the occurrence of central scattering suggests the existence of scattering objects in the films. These objects are polymer/air interfaces (PE for PE-1 samples and polypyrrole for the composite). It should be noted that, for the starting and composite films, central scatterings differ significantly, whereas scatterings at large angles are almost coincident. This is indicative of the fact that the structure of the films with sizes of 10 nm or lower remained unchanged in the course of preparing the composite. Most likely, its porous structure having sizes above 10 nm has changed.

Corresponding size volume distributions of scattering objects in these films are presented in Fig. 13. The distribution curves were plotted via two independent methods in order to eliminate the ambiguity of polydispersity determination for the samples in question. Curves 1 and 2 constitute size distributions for the starting PE film and the composite film sample, respectively. These curves were computed with the use of the

indirect Fourier transform according to the GNOM program [21]. The dashed and solid lines represent distributions for the same films but resulting from the direct simulation of scattering curves by a system of polydisperse spheres (the POLYMIX program [22]). Volume distribution functions calculated by the two methods practically coincide, thereby confirming the reliability of the calculation results.

An analysis of the $D_V(R)$ profiles shows that, after filling of PE pores with polypyrrole, their size

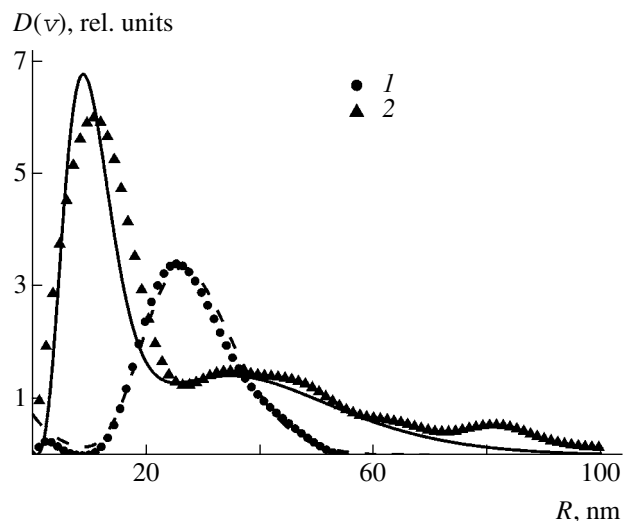


Fig. 13. Size volume distributions $D(v)$ for the starting polymer and the composite computed via different methods: points 1 (the starting polymer) and 2 (PE-1-based composite containing 24.2% polypyrrole) are calculated by the GNOM program [21]; dashed and solid lines refer to corresponding distributions obtained by the POLYMIX program [22].

decreased on average by a factor of 3 as early as after the first synthesis of the conducting polymer. Furthermore, the character of pore distribution changes sharply. The starting microporous PE is characterized by an almost unimodal distribution with basic sizes of the order of 30 nm. In the case of the composite, not only the basic maximum shifts to pore sizes of 10 nm but also a significant amount of large pores having sizes up to 100 nm and a maximum near 40 nm appear. It is suggested that the rigid-chain polypyrrole formed inside the elastic PE support causes its deformation. As a result, the pores widen and the number of scattering objects grows. Previous filtration porosimetry studies [23] revealed that larger scattering objects are present that are however undetectable at wavelengths employed in SAXS measurements.

CONCLUSIONS

In summary, we developed and first carried out the synthesis of polypyrrole–microporous PE composites through polymerization of pyrrole in supercritical carbon dioxide. The method is distinguished by easiness and ecological safety. It was shown that the multi-step successive synthesis on the PE films offers a convenient technique for the growth and control over the thickness of the polypyrrole layer on the surface and in the bulk of the microporous PE. It was shown that the polymers entering into the composite composition show good adhesion compatibility (up to a polypyrrole content of ~40%). The possibility of obtaining composites with a high content of the electroconductive component (up to ~50% polypyrrole) was demonstrated.

Spectroscopic studies of the polymer composites under consideration testified that, during the synthesis in supercritical CO₂, as during polymerization performed by other methods (in solution [31] or in the gas phase [18]), with the use of ferric trichloride as an oxidizer, the oxidized (conductive) form of polypyrrole is formed.

REFERENCES

1. H. Shirakawa, E. J. Louis, A. G. McDiarmid, et al., *J. Chem. Soc., Chem. Commun.*, 578 (1977).
2. T. V. Vernitskaya and O. N. Efimov, *Usp. Khim.* **66**, 489 (1997).
3. *Handbook of Organic Conductive Molecules and Polymers*, Ed. by H. S. Nalwa (Wiley, Chichester, 1997), Vol. 2.
4. J. Yang, J. Hou, W. Zhu, et al., *Synth. Met.* **80**, 283 (1996).
5. D. L. Feldheim and C. M. Elliott, *J. Membr. Sci.* **70**, 9 (1992).
6. K. L. Levin, V. N. Zgonnik, and V. I. Frolov, *Vysokomol. Soedin., Ser. B* **35**, 1702 (1993) [*Polymer Science, Ser. B* **35**, 1425 (1993)].
7. T. Sata, *J. Phys. Chem.* **97**, 6920 (1993).
8. E. Yu. Rozova, G. A. Polotskaya, A. G. Kozlov, et al., *Vysokomol. Soedin., Ser. A* **40**, 914 (1998) [*Polymer Science, Ser. A* **40**, 530 (1998)].
9. G. K. Elyashevich, E. Yu. Rosova, and I. S. Kuryndin, *Desalination* **144**, 21 (2002).
10. A. I. Cooper, *J. Mater. Chem.* **10**, 207 (2000).
11. S. G. Kazarian, *Polymer Science, Ser. C* **42**, 78 (2000).
12. M. Perrut, *Ind. Eng. Chem. Res.* **39**, 4531 (2000).
13. F. M. Kerton, G. A. Lawless, and S. P. Armes, *J. Mater. Chem.* **7**, 1965 (1997).
14. Y. Fu, D. R. Palo, C. Erkey, and R. A. Weiss, *Macromolecules* **30**, 7611 (1997).
15. S. L. Shenoy, D. Cohen, R. A. Weiss, and C. Erkey, *J. Supercrit. Fluids* **28**, 233 (2004).
16. L. Nikitin, E. Said-Galiyev, R. Vinokur, et al., in *Proceedings of 8th Meeting on Supercritical Fluids, Bordeaux, 2002*, Vol. 1, p. 213.
17. L. Nikitin, A. Nikolaev, G. Elyashevich, et al., in *Proceedings of 3rd International Symposium on Supercritical Fluid Technology for Energy and Environment Applications, China, 2004*, p. 38.
18. G. K. Elyashevich, V. K. Lavrentyev, I. S. Kuryndin, and E. Yu. Rosova, *Synth. Met.* **119**, 277 (2001).
19. G. K. Elyashevich, A. E. Bitskii, A. G. Kozlov, and E. Yu. Rozova, *Zh. Prikl. Khim. (S.-Peterburg)* **70**, 1175 (1997).
20. A. S. Filonov, D. Yu. Gavrilko, and I. V. Yaminskii, *Program Package "FemtoScan" for Three-Dimensional Image Processing* (Tsentr Perspekt. Tekhnol., Moscow, 2001) [in Russian].
21. D. I. Svergun, *J. Appl. Crystallogr.* **25**, 495 (1992).
22. P. V. Konarev, V. V. Volkov, A. V. Sokolova, et al., *J. Appl. Crystallogr.* **36**, 1277 (2003).
23. G. K. Elyashevich, A. G. Kozlov, and E. Yu. Rozova, *Vysokomol. Soedin., Ser. A* **40**, 956 (1998) [*Polymer Science, Ser. A* **40**, 567 (1998)].
24. G. K. Elyashevich, A. G. Kozlov, and I. T. Moneva, *Vysokomol. Soedin., Ser. B* **40**, 483 (1998) [*Polymer Science, Ser. B* **40**, 71 (1998)].
25. A. G. Kozlov, I. S. Kuryndin, E. Yu. Rozova, and G. K. Elyashevich, *Vysokomol. Soedin., Ser. A* **42**, 425 (2000) [*Polymer Science, Ser. A* **42**, 279 (2000)].
26. M. Raab, J. Scudla, A. G. Kozlov, et al., *J. Appl. Polym. Sci.* **80**, 214 (2001).
27. G. K. Elyashevich, E. Yu. Rosova, A. V. Sidorovich, et al., *Eur. Polym. J.* **39**, 647 (2003).
28. Y. Furukawa, S. Tazawa, Y. Fujii, and I. Harada, *Synth. Met.* **24**, 329 (1988).
29. A. M. Timonov and S. V. Vasil'eva, *Sorosovskii Obrazov. Zh.* **6** (3), 33 (2000).
30. *AIST Raman Spectra Database of Minerals and Inorganic Materials, 2004*. http://www.aist.go.jp/RIODB/rasmin/E_index.htm.
31. M. A. Smirnov, N. V. Bobrova, Z. Rientka, and G. K. Elyashevich, *Vysokomol. Soedin., Ser. B* **47**, 1231 (2005) [*Polymer Science, Ser. B* **47**, 215 (2005)].